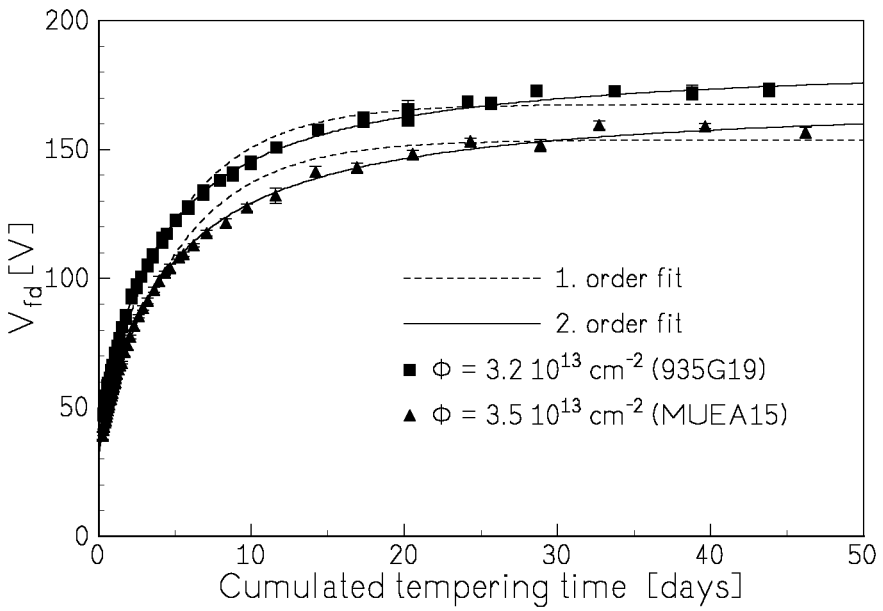

Figure 6.3: Comparison of fits due to 1 order (eq. 6.8) and 2 order (eq. 6.9) assumption. Samples were tempered at 50 °C.

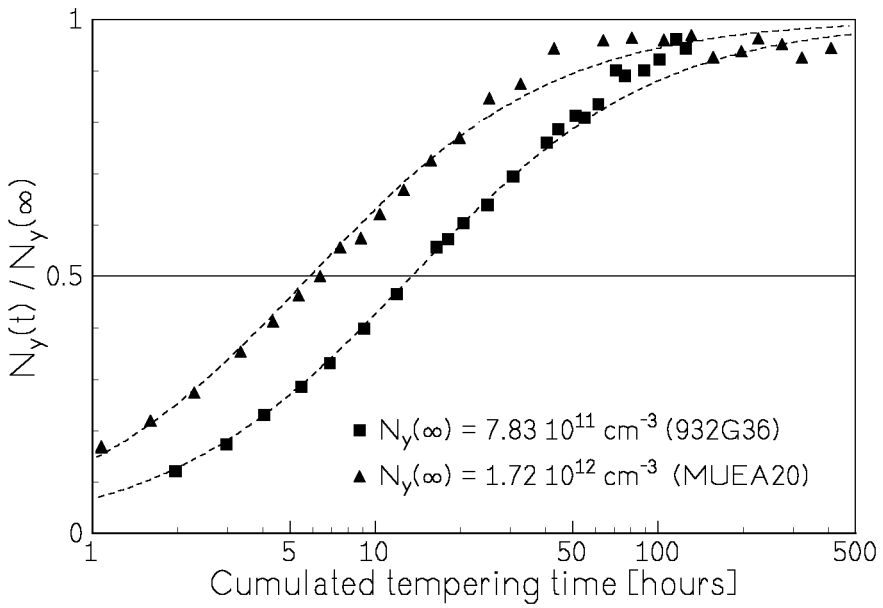

Figure 6.4: Comparison of half-life period. Samples were tempered at 70°C.

A comparison of first and second order models has already been performed by Sotthibandu [119]. The room temperature annealing of samples irradiated in a fluence range between $2{\cdot}10^{13}$ cm^{-2} and $1.6{\cdot}10^{14}$ cm^{-2} has been fitted to both models. It was found that the time constants $1/\hat{k}$ obtained from the first order fits clearly decrease with fluence (from 370 days down to 70 days). This behaviour is equivalent to a fluence dependent half-life period. The rate constants obtained from the second order fits were independent of the fluence. The average value is $\tilde{k} = 3.1{\pm}1.2\ 10^{-20}$ cm^3/s and in good agreement with the result of this work (see sec. 6.1.2.4).

To determine the fluence and time dependence of the reverse annealing, the technique of isothermal heat treatment has mainly been used. The behaviour of ΔN_{eff} as function of time at room temperature and during the following heat treatment at 50°C is demonstrated in fig. 6.5. Disregarding all short term annealing effects

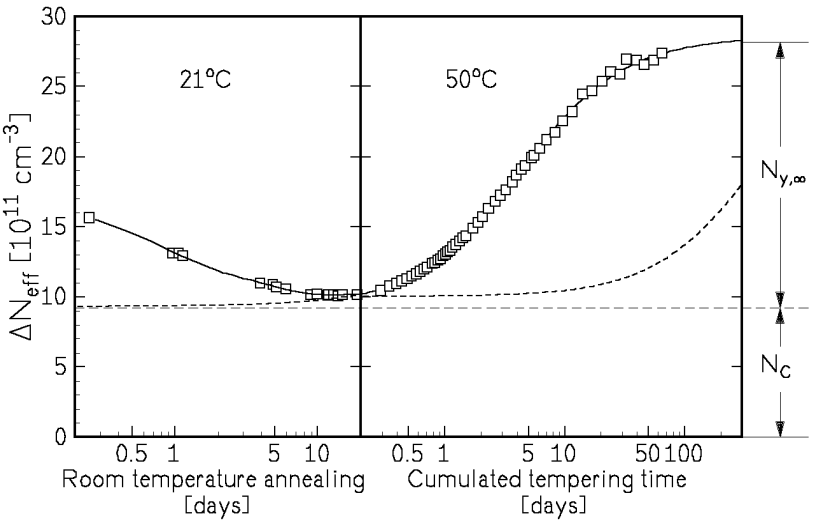

Figure 6.5: Development of ΔN_{eff} before and during heat treatment. The broken line presents the expected room temperature annealing.

ΔN_{eff} can be written as a sum of two components N_C and N_Y :

$$\Delta N_{eff}(t) = N_Y(t) + N_C. \tag{6.10}$$

$N_Y(t)$ is the concentration of the defect which causes the reverse annealing and the concentration N_C summarises all electrically active defects which remain constant in time. Combining eqs. 6.9 and 6.10 one gets the full expression to fit $\Delta N_{eff}\ (t)$:

$$\Delta N_{eff}(t) = N_{X,0}\left(1 - \frac{1}{1 + N_{X,0}\tilde{k}t}\right) + N_C. \tag{6.11}$$

From each isothermal heat treatment a set of parameters $N_{Y,\infty}$, $(= N_{X,0})$, $\tilde{k}$ and N_C has been determined by a 'least squares fit'. The annealing time of all samples used for the analysis of $N_{Y,\infty}$ and $\tilde{k}$ exceeds the half-life period. In the following firstly

the fluence dependence of $N_{Y,\infty}$ and N_C is discussed in (sec. 6.1.2.2, sec. 6.1.2.3) and secondly in sec. 6.1.2.4 several aspects of the rate constant $\tilde{k}$ are deliberated. The results are then compared to those obtained from samples annealed at lower temperature ($T < RT$) sec. 6.1.2.5.

Finally, after confirmation of the second order model by the results of the isochronal heat treatments some aspects of the microscopic structure of the model are discussed sec. 6.1.2.7.

Because after a heat treatment the depletion voltage declines with a time constant of about 6 hours, all measurements of depletion voltages used for the analysis of the reverse annealing were not performed before a constant value was reached. A detailed description of this effect is given in sec. 6.1.2.8.

6.1.2.2 Fluence Dependence of $N_{Y,\infty}$

As can be seen from fig. 6.6 $N_{Y,\infty}$ increases linearly with fluence up to $\Phi = 1.2{\cdot}10^{14}$ cm^{-2} :

$$N_{Y,\infty}(\Phi) = b_Y \Phi. \tag{6.12}$$

No difference can be observed between the data obtained from samples which were completely reverse annealed at elevated temperatures and the data from the room temperature annealing, although the reverse annealing was not completed for any of the room temperature samples. The generation rate is found to be

$$b_Y = 0.0527 \pm 0.0063 \text{ cm}^{-1}$$

independent of the detector type or geometry as it is shown in fig. 6.7. Neither the p-type sample (from wafer 936) nor the p$^+$-n diodes (MUE) deviate from the n-type SB-detectors. Similar generation rates have been found by other authors using the first order assumption [36, 120, 121, 122]. Also data taken from proton irradiated SB-detectors samples are consistent with the value given above [67].

6.1.2.3 Fluence Dependence of N_C

The concentration of electrically active defects C which is constant in time after irradiation exhibits a more complicated fluence dependence than N_Y. As can be seen from fig. 6.8 N_C depends linearly on Φ only at fluences above $1{\cdot}10^{13}$ cm^{-2}. From the slope a generation rate b_C can be determined. At lower fluences it is more likely to fit the data using an exponential term $(1 - \exp(-c_C\Phi))$ with an amplitude $N_{C,0}$. In total the fluence dependence of N_C is described by the following equation :

$$N_C(\Phi) = N_{C,0}(1 - \exp(-c_C\Phi)) + b_C\Phi, \tag{6.13}$$

and the parameters are found to be

$$\begin{aligned} N_{C,0} &= 3.36\ (\pm\ 0.03)\ {\cdot}10^{11}\ \text{cm}^{-3}, \\ c_C &= 3.58\ (\pm\ 0.20)\ {\cdot}10^{-13}\ \text{cm}^2 \text{ and} \\ b_C &= 0.0171 \pm 0.0001\ \text{cm}^{-1}. \end{aligned}$$

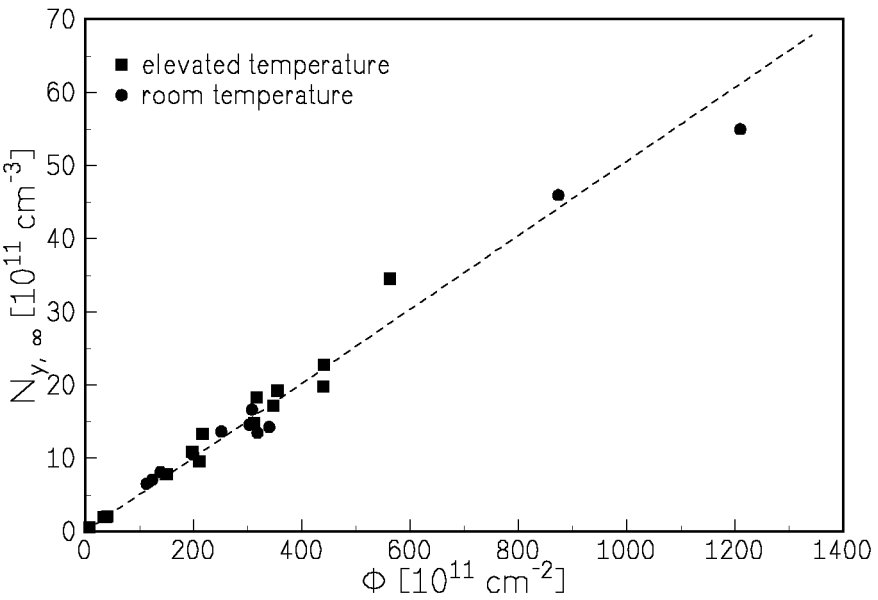

Figure 6.6: The maximum defect concentration of reverse annealing $N_{Y,\infty}$ versus fluence. Reverse annealing at elevated temperature has been completed, at room temperature the minimum annealing time exceeded the half-life period $t_{1/2} = 1/N_{X,0}\tilde{k}$ (see sec. 3.2).

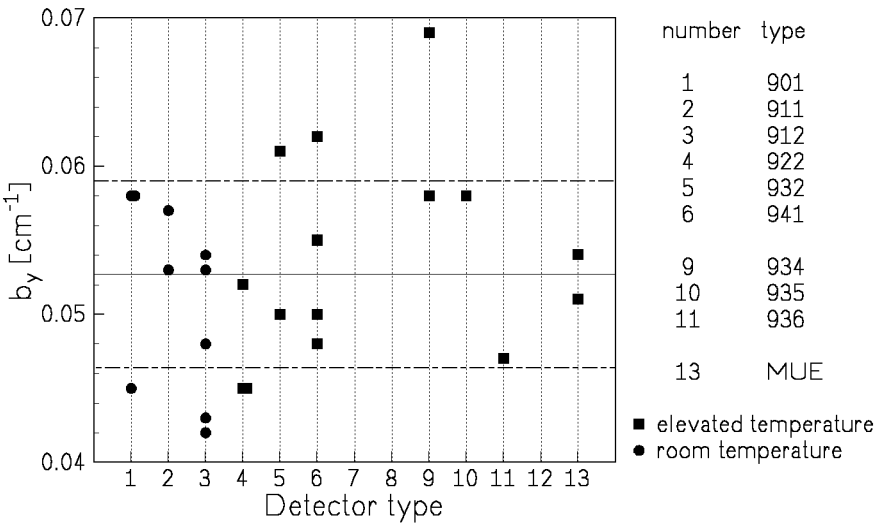

Figure 6.7: Introduction rate b_Y of various detector types. See tab. 5.1 for explanation of individual properties. The average value $b_Y = 0.0527 \pm 0.0063$ cm^{-1} is marked by the solid line, the standard deviation by the broken line.

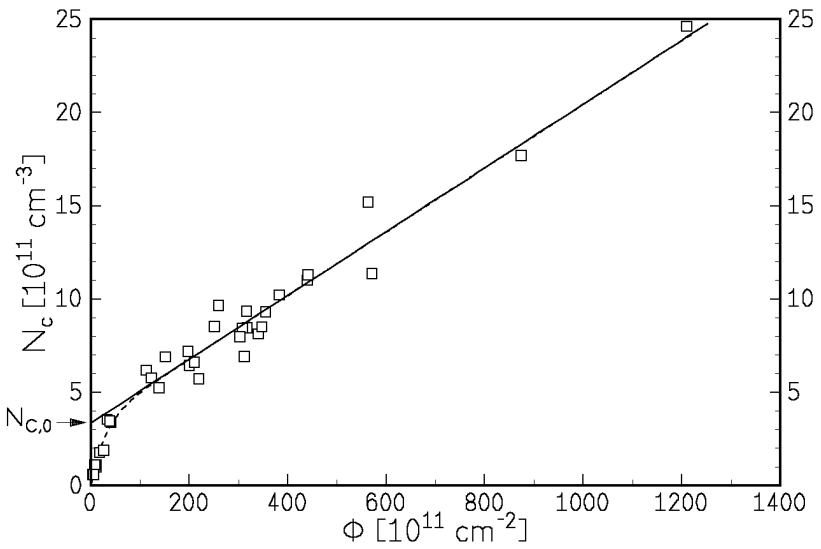

Figure 6.8: Concentration of constant defects N_C versus fluence. Fit according to eq. 6.13

The same parametrisation as for $N_C(\Phi)$ yields for $\Delta N_{eff}(\Phi)$ which can be deduced from eqs. 6.1 and 6.2 :

$$\Delta N_{eff}(\Phi) = N_{D,0}(1 - \exp(-c\Phi)) + b_A\Phi. \tag{6.14}$$

Both functions are plotted in fig. 6.9. Because ΔN_{eff} (Φ) describes the radiation induced change of the impurity concentration corrected for self annealing and N_C the non-annealing fraction, the gap between both curves represents the fraction of annealing defects. Because the values of c_D $(= 3.54{\cdot}10^{-13}$ cm^2, see tab. 6.1) and c_C are equal it can be concluded that in both cases the same phenomenon, e.g. donor removal, is described. Then from a comparison of $N_{D,0}$ and $N_{C,0}$ one gets the ratio of recovered donors and those which are definitely removed. This conclusion implies $N_{C,0}$ to be dependent on the initial phosphorus concentration. However, due to the lack of adequate information about the phosphorus concentration in the samples under investigation, only the dependence of $N_{C,0}$ on $N_{eff,0}$ can be given. In fig. 6.10 the individual $N_{C,0}$:

$$N_{C,0} = N_C - b_C\Phi \tag{6.15}$$

of samples irradiated with a fluence $\Phi > 1.5{\cdot}10^{13}$ cm^{-2} is plotted versus the effective doping concentration before irradiation. The obvious correlation confirms the assumption made above. The difference between the values found for b_C and b_A $(= 7.94{\cdot}10^{-2}$ cm^{-1}, see tab. 6.1) represents the annealed fraction of the radiation induced acceptor concentration.

Comparing the generation rate b_C and g_{Mg} (see sec. 3.1) it can be seen that both have similar values, 0.02 cm^{-1} and 0.01 cm^{-1} respectively. However, magnesium is a donor and contributes a positive charge, whereas the defects summarised in the concentration N_C are obviously negatively charged acceptor-states.

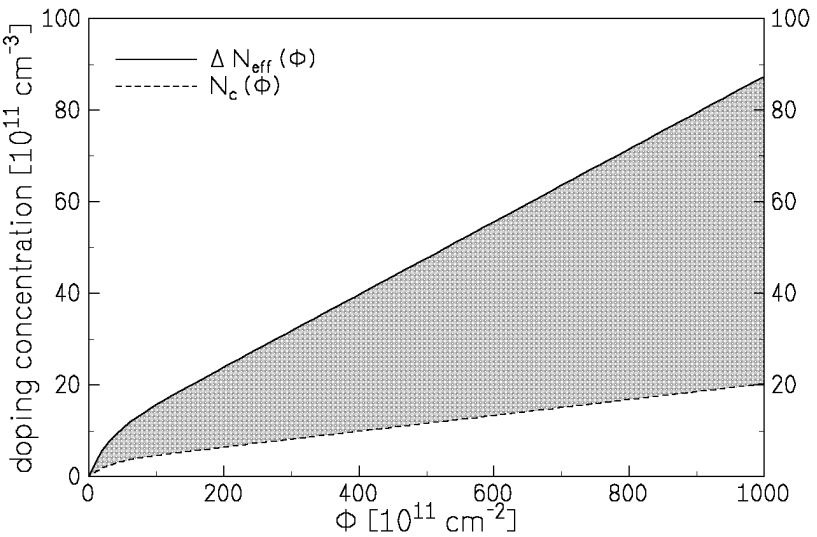

Figure 6.9: Comparison of fluence dependence of ΔN_{eff} and N_C. $N_{D,0} = 8{\cdot}10^{11}$ cm^{-3}, $N_C = 3{\cdot}10^{11}$ cm^{-3}.

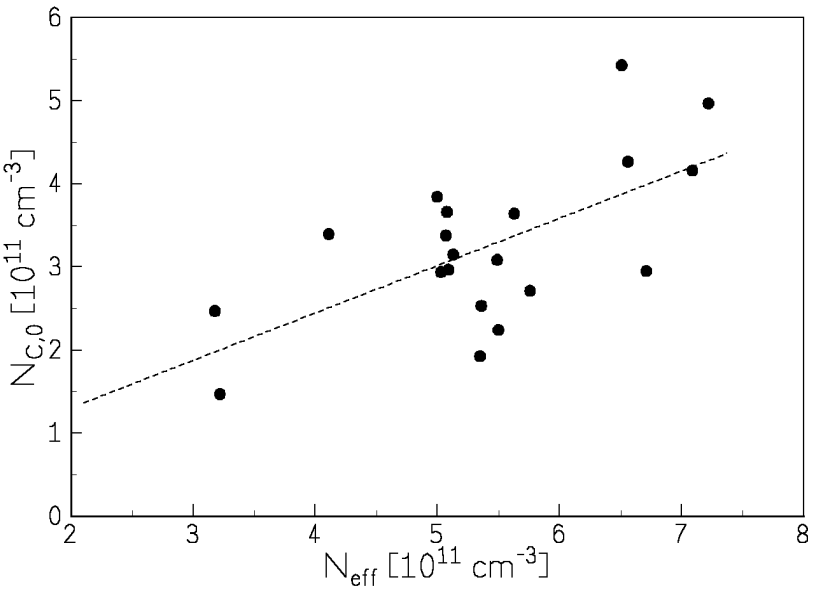

Figure 6.10: $N_{C,0}$ versus $N_{eff,0}$.

6.1.2.4 The Second Order Rate Constant

The third parameter obtained by fitting the data of an isothermal heat treatment is the reaction constant $\tilde{k}$. Only data obtained from samples irradiated in the fluence range $1{\cdot}10^{13}$ cm$^{-2} < \Phi < 5{\cdot}10^{13}$ cm^{-2} were used to determine the activation energy E_a and the frequency factor $\tilde{k}_o$, because the reaction constant depends weakly on

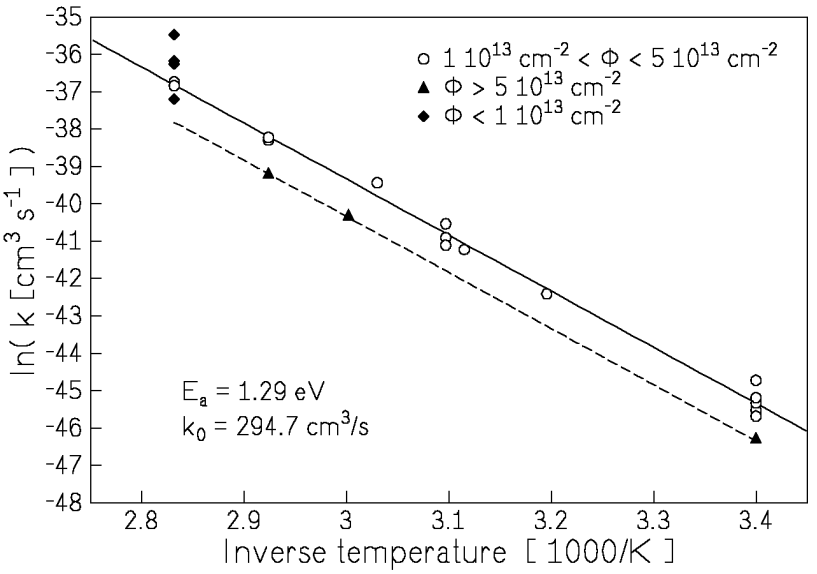

Figure 6.11: Arrhenius plot of second order reaction constant $\tilde{k}$. Data marked by filled symbols are excluded from analysis (see text).

the fluence.

In fig. 6.12 the reaction constants $\tilde{k}(21°\mathrm{C})$ and $\tilde{k}(80°\mathrm{C})$ are plotted versus neutron fluence. For comparison data of proton irradiated samples annealed at 80°C are also shown [67]. Although the data are fluctuating, for both temperatures a straight line has been fitted to the data to demonstrate that $\tilde{k}$ decreases slightly with fluence. However, due to the strong fluctuation an exact parametrisation seems to be unlikely and hence the average value of data from the fluence range given above is calculated :

$$\begin{aligned} \tilde{k}(21°\mathrm{C}) &= 1.9\pm0.4\ 10^{-20}\ \mathrm{cm}^3\ \mathrm{s}^{-1}, \text{ and} \\ \tilde{k}(80°\mathrm{C}) &= 2.3\pm1.6\ 10^{-16}\ \mathrm{cm}^3\ \mathrm{s}^{-1}. \end{aligned}$$

Using the Arrhenius relation (eq. 4.78) it was found that E_a=1.29 eV and $\tilde{k}_o$=294.7 $\mathrm{cm}^3\mathrm{s}^{-1}$ (see fig. 6.11). The rate constants obtained from the strong irradiated samples can obviously be described by the same activation energy, but a lower frequency factor. A meaningful physical interpretation of this finding could not be found so far.

6.1.2.5 Reverse Annealing at Lower Temperature

Three sets of samples (see tab. 6.3) were irradiated and stored at temperatures below room temperature for up to 8 months. Each set consisted of three detectors of different suppliers : SB-detectors from Hamburg and p^+-n -detectors from Micron and Intertechnique (see sec. 5.1). Comparing fig. 6.13 a.) - c.) it can be seen that the increase of N_{eff} above the minimum becomes less steep at lower temperatures. At 6°C only a very small increase can be observed at all. Hence it seems to be unlikely to fit the development of N_{eff} to eq. 6.11 by using 3 free parameters and thus only

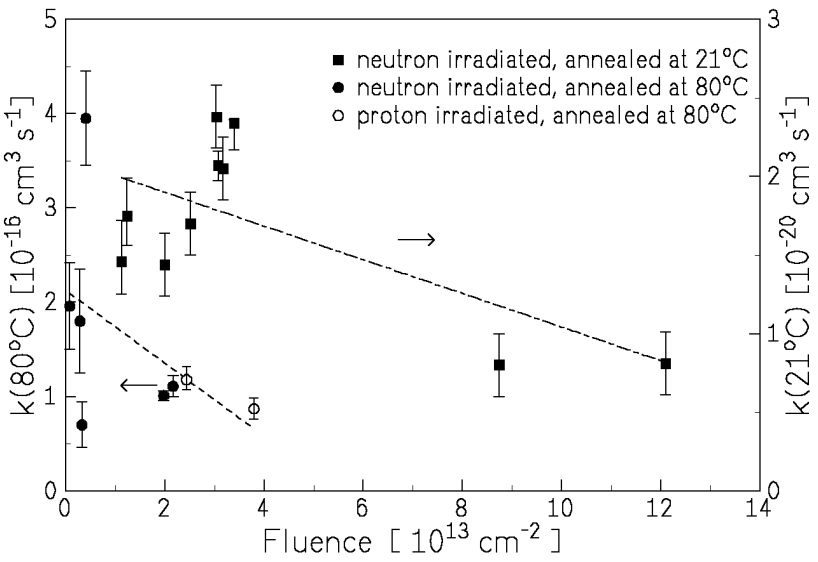

Figure 6.12: Second order reaction constant $\tilde{k}(80°\mathrm{C})$ and $\tilde{k}(21°\mathrm{C})$ versus fluence. The empty symbols are for data taken from proton irradiated samples.

N_C and $\tilde{k}$ were fitted. $N_{X,0} = N_{Y,\infty}$ was calculated using the generation rate $b_Y = 0.0527\ \mathrm{cm}^{-1}$, because it is independent of both the detector type and the fluence (see sec. 6.1.2.2). In order to be far enough from the minimum of the annealing curve even for the values taken at 6°C only data $N_{eff}(t)$ for $t > 1.5{\cdot}10^5$ min (97 days) after irradiation were fitted. The results of the fits are summarised in tab. 6.3.

The values obtained for N_C agree very well with $N_C(\Phi)$ as calculated from eq. 6.13 and the parameters given in sec. 6.1.2.3[2] Thus the concentration of electrically active defects which is constant in time after irradiation is independent of the temperature.

The reaction constants $\tilde{k}$ are plotted in fig. 6.13. The straight line represents $\tilde{k}(T)$ as expected from the results of the heat treatments. Additionally the values of $\tilde{k}$ at room temperature are shown and it can be seen that the deviation of the low temperature values from the straight line is comparable to the fluctuation of the room temperature values.

Thus the good agreement of both parameters, N_C and $\tilde{k}$ with the prediction of the second order model also justifies its application in the temperature range 0°C - 20°C.

6.1.2.6 Results of Isochronal Heat Treatments

Isochronal heat treatments were applied to two samples (see tab. 6.4) in order to prove consistency with the results obtained from the isothermal heat treatments.

For demonstration the development of the effective doping concentration of one of the samples is shown in fig. 6.14. The first annealing step between 50°C and

[2] $N_C(2.75{\cdot}10^{12}\ \mathrm{cm}^{-2}) = 8.06{\cdot}10^{11}\ \mathrm{cm}^{-3}$ and $N_C(2.95{\cdot}10^{12}\ \mathrm{cm}^{-2}) = 8.40{\cdot}10^{11}\ \mathrm{cm}^{-3}$.

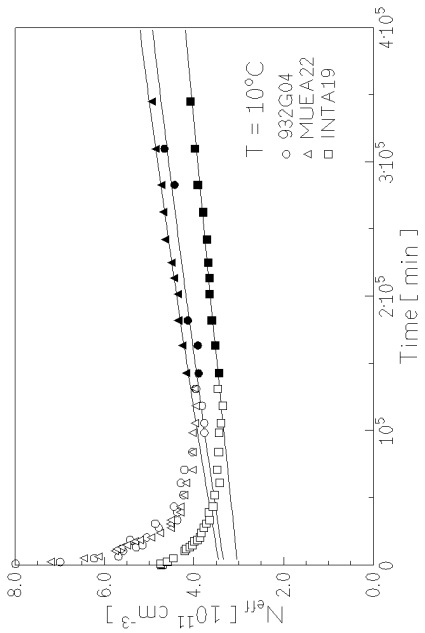
T = 10°C
○ 932G04
△ MUEA22
□ INTA19
N_{eff} [10^{11} cm^{-3}]
Time [min]

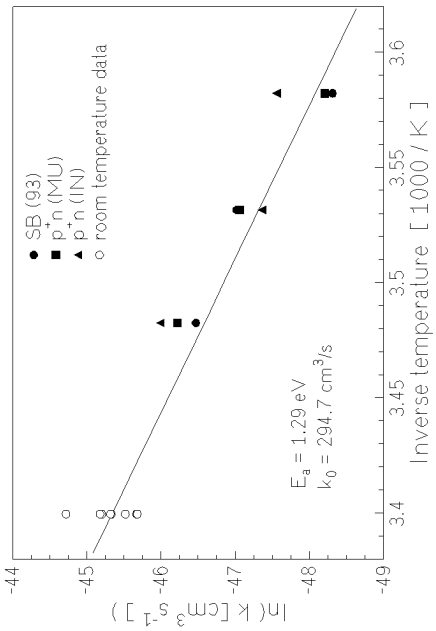
● SB (93)
■ p^+n (MU)
▲ p^+n (IN)
○ room temperature data
E_a = 1.29 eV
k_0 = 294.7 cm^3/s
ln(K [cm^3 s^{-1}])
Inverse temperature [1000 / K]

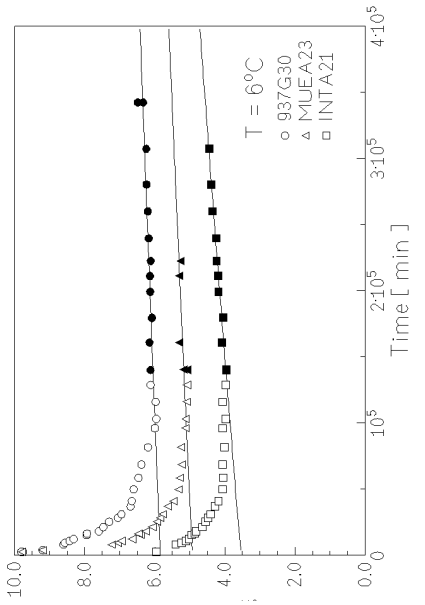
T = 6°C
○ 937G30
△ MUEA23
□ INTA21
Time [min]